Research in Astronomy and Astrophysics, 24:125014 (18pp), 2024 December https://doi.org/10.1088/1674-4527/ad8f9b

Spectroscopic Study of Late-type Emission-line Stars Using the Data from LAMOST DR6

D. Edwin[1], Blesson Mathew[1], B. Shridharan[1,2], Vineeth Valsan[1], S. Nidhi[1,3], Suman Bhattacharyya[1], Sreeja S. Kartha[1], and T. Robin[1]

[1] Department of Physics and Electronics, CHRIST (Deemed to be University), Hosur Main Road, Bangalore, 560029, India; blesson.mathew@christuniversity.in, edwin.jv@res.christuniversity.in

[2] Department of Astronomy and Astrophysics, Tata Institute of Fundamental Research, Mumbai, 400005, India

[3] The Oxford College of Science, 17th, 32, 19th Main road, Sector 4, HSR Layout, Bengaluru, Karnataka, 560102, India

Received 2024 May 27; revised 2024 October 6; accepted 2024 October 17; published 2024 December 4

Abstract

Low-mass emission-line stars belong to various evolutionary stages, from pre-main-sequence young stars to evolved stars. In this work, we present a catalog of late-type (F0 to M9) emission-line stars from the LAMOST Data Release 6. Using the `scipy` package, we created a Python code that finds the emission peak at Hα in all late-type stellar spectra. A data set of 38,152 late-type emission-line stars was obtained after a rigorous examination of the photometric quality flags and the signal-to-noise ratio of the spectra. Adopting well-known photometric and spectroscopic methods, we classified our sample into 438 infrared (IR) excess sources, 4669 post-main-sequence candidates, 9718 Fe/Ge/Ke sources, and 23,264 dMe sources. From a crossmatch with known databases, we found that 29,222 sources, comprising 65 IR excess sources, 7899 Fe/Ge/Ke stars, 17,533 dMe stars, and 3725 PtMS candidates, are new detections. We measured the equivalent width of the major emission lines observed in the spectra of our sample of emission-line stars. Furthermore, the trend observed in the line strengths of major emission lines over the entire late-type spectral range is analyzed. We further classified the sample into four groups based on the presence of hydrogen and calcium emission lines. This work presents a large data set of late-type emission-line stars, which can be used to study active phenomena in late-type stars.

Key words: Stars: late-type – Stars: activity – Line: identification

1. Introduction

The emission of Hα is frequently observed in active pre- and post-main-sequence (PtMS) stars, as well as in binary stars. The investigation of stars exhibiting Hα emission holds considerable physical significance. Historically, the study of these stars commenced in the early 1940s where Merrill & Burwell (1933) published their work on spectroscopic observations of Hα emission stars in the northern Milky Way, which sparked interest in emission-line stars (ELS). Following this, Bidelman (1954) compiled a catalog of stars later than spectral type B, which showed emission in Hα and Ca II H and K. Wray (1966) and Henize (1976) conducted research on Hα emission stars in the southern Milky Way, which further helped in expanding our understanding of ELS. In the 1980s, multiple surveys such as MacConnell (1981), Stephenson (1986), and Wiramihardja et al. (1989) extensively studied ELS in different parts of our galaxy. In subsequent years, ELS were also surveyed and identified beyond our galaxy, notably from the Large Magellanic Cloud (LMC; Bohannan 1987) and Small Magellanic Cloud (SMC; Meyssonnier & Azzopardi 1993; Le Coarer et al. 2005; Martayan et al. 2010).

The advent of the Sloan Digital Sky Survey (SDSS; York et al. 2000) has contributed to the field of stellar spectroscopy and improved the understanding of various active phenomena in stars. Also, the Isaac Newton Telescope (INT) Photometric Hα Survey (IPHAS; Drew et al. 2005), a program that used broad-band *r* and *i*, and narrow-band Hα filters, studied the northern plane of our galaxy. One of the specific goals of this survey program was to study the young stellar objects (YSOs) in our galaxy (Barentsen et al. 2014). The Gaia-ESO survey (Traven et al. 2015), which studied the spectra of a number of active ELS, also improved the list of ELS. These build a great foundation for the upcoming studies and surveys on ELS in our galaxy. Furthermore, RAdial Velocity Experiment (RAVE; Steinmetz 2002), an all-sky spectroscopic survey to measure stellar parameters like radial velocity, metallicity, and abundance ratios of 50 million stars in our galaxy, contributed much to the understanding of ELS research.

The study of ELS in the low-mass regime is critical due to the occurrence of a diverse range of active phenomena in these sources. Late-type emission-line stars (LELS) are low-mass ($<3\,M_{\odot}$) ELS belonging to spectral types F0 to M9. LELS can be broadly classified into infrared (IR) excess sources, Fe/Ge/Ke/dMe (main-sequence) stars, and PtMS candidates. Classical T Tauri stars (CTTSs) are YSOs that undergo accretion, with Hα emission

originating primarily from the accretion columns and the circumstellar disk (Kurosawa et al. 2005). These stars exhibit significant IR excess. In main-sequence Ge/Ke/dMe stars, the Hα emission occurs from the chromosphere of the star, which is usually attributed to the large-scale magnetic fields observed in low-mass stars (Hall 2008). In PtMS F- and G-type stars, Hα originates from the expanding outer shell and ejected material (Kogure & Leung 2010). In stars like Mira variables, the origin of the emission lines is due to the pulsations leading to the generation of shock waves, which results in intense emission lines in their spectra (Wood 1979; Gillet et al. 1983; Kogure & Leung 2010). Hence, the primary objective of this work is to classify LELS into distinct evolutionary stages.

The major emission lines observed in the optical spectra of late-type stars include Ca II H and K, Hα, and the Ca II triplet (CaIRT). Most of these lines are often linked with chromospheric activity in low mass stars (Cincunegui et al. 2007; Smith 2011). Other factors that influence the strength and profile shape of the emission lines are due to stellar rotation, age of the star, wind, and magnetic field. Multiple photometric (Radick et al. 1983; Herbst & Miller 1989; Lockwood et al. 2007) and spectroscopic (Gizis et al. 2002; López-Santiago et al. 2010; Suárez Mascareño et al. 2015) studies provided us with good insights on different groups of LELS in our galaxy. Notably, utilizing SDSS spectra, West et al. (2004) studied the magnetic properties of cool stars, where they used emission in Hα as the primary indicator of activity. Also, RAVE studies on 38,000 chromospherically active solar-type stars in the solar neighborhood were carried out by Žerjal et al. (2017).

Large Sky Area Multi-Object Fiber Spectroscopic Telescope (LAMOST) has provided a huge spectral database for the scientific community, containing more than 10 million low-resolution spectra of stars, galaxies, and QSOs. There are several works that have used the LAMOST database to study different types of LELS, such as Mira variables (Yao et al. 2017), M dwarfs (Yi et al. 2014; Guo et al. 2015; Chang et al. 2017) and M-giants (Liu et al. 2014; Zhong et al. 2015; Li et al. 2019). The present study complements the work of Shridharan et al. (2021), where they created a catalog of early-type ELS using the spectra available in LAMOST data archive. We queried the entire LAMOST spectral database for sources classified as F, G, K, and M spectral types and identified the spectra showing the Hα emission line. We then classify our sample into Fe/Ge/Ke/dMe stars, PtMS candidates, and YSOs on the basis of their photometric and spectroscopic features. It improves the existing sample of LELS, in turn opening the gateway for studying interesting low-mass sources in our galaxy and improving our understanding on the chromospheric, rotational, magnetic, and all other kinds of activity in these sources.

In this work, we catalog 38,152 LELS into their various categories and study their spectral characteristics. In Section 2, we describe the data collection method utilized for our work. In Section 3, we provide a brief description on different classes of LELS and the classification criteria utilized in classifying our sample. In Section 4, the results of this work that contain different types of LELS are separated, and their properties and characteristics are described. The conclusion is provided in Section 5.

2. Data Collection and Compilation

2.1. Identification of late-type Stars from LAMOST DR6 Spectral Database

LAMOST is a reflecting Schmidt telescope (Zhao et al. 2012), observing a field of view (FoV) of 20 deg^2 (Sun et al. 2021) in the sky. By 2018 July, LAMOST had released its sixth data release (DR6), observing 9,911,337 low-resolution spectra (LRSs). They were subdivided into four categories, namely "STAR," "GALAXY," "QUASAR," and "unknown" spectra. Among the four categories, over 90% of the LRSs belong to the "STAR" category. A typical LRS contains calibrated wavelengths on the x-axis and flux on the y-axis, with a wavelength range of 3690 Å–9100 Å and a resolution of 1800 at 5500 Å (Zhao et al. 2012; Yan et al. 2022). The survey spans a decl. range of $= -10°$ to $+90°$ (Deng et al. 2012).

For the present work, we have restricted the analysis to a sample of F, G, K, and M spectral types. Hence, we queried these stars in the LAMOST DR6 (LDR6) catalog and obtained more than 1.7 million star spectra belonging to F type, ∼2.9 million G-type spectra, ∼1 million K-type spectra, and ∼0.55 million M-type spectra. The general catalog of LDR6 contains 37 columns worth of data including the stars' positions, error estimates, identifiers, and magnitudes in u, g, r, i, and z bands, redshift, etc. (Wu et al. 2014). The LRS A, F, G, K type star catalog has, along with the general catalog data, information on effective temperature ($T_{\rm eff}$), surface gravity (log(g)), metallicity [Fe/H], heliocentric radial velocity (rv), and their corresponding errors. These parameters are estimated by the LAMOST parameter pipeline (LASP) (Wu et al. 2014). The LRS M-type star catalog has estimated the parameters mentioned in the previous catalog using the cross-correlation method. Furthermore, the catalog provides additional information, which includes Hα equivalent width (EW) and the line indices (TiO, CaH, CaOH, Na) estimated using the HAMMER software (Liu et al. 2014).

2.2. Selection of Late-type Emission-line Stars

Initially, 8,613,834 F-, G-, K-, and M-type spectra labeled as STAR were queried from the LDR6[4] and the spectra were continuum normalized using the `laspec` package[5] (Zhang et al. 2020). Using the `scipy.signal.findpeaks`[6] parameter, a Python routine was developed to inspect for the

[4] www.lamost.org/dr6
[5] https://github.com/hypergravity/laspec
[6] https://docs.scipy.org/doc/scipy/reference/generated/scipy.signal.find_peaks.html

presence of Hα emission in the sample (Shridharan et al. 2021). The parameter "width" was utilized to avoid false emission sources, and only the sources with width greater than three sampling points were considered as detections. This avoided narrow peaks caused by instrumental noise or defects. If the spectra do not show Hα in emission, they are removed from further analysis. As a result, we obtained 80,860 spectra with the Hα emission line within 3 Å of 6563 Å. Only stars having signal-to-noise ratio (SNR) in `r` band (SNR$_r$) greater than 10 are further considered for the study, and the rest are eliminated, leaving us with a sample of 58,508 LELS spectra. We further separated the sources having LELS spectra with SNR $(x) = -9999$ (where x represents u, g, r, i, and z bands). Those spectra were considered "BAD spectra" upon visual check and removed from this study, which left us with a sample of 56,291 spectra belonging to 48,657 unique sources. Furthermore, we utilized the `line_index` function of the `laspec` package to estimate the EW of major emission lines for all the sources in our study.

2.2.1. Crossmatch with Photometric Catalogs

In order to characterize the identified Hα source, we obtain photometric values from various optical/IR all-sky surveys such as Two Micron All-Sky Survey (2MASS) (Skrutskie et al. 2006), Gaia (Prusti et al. 2016; Vallenari et al. 2023), and Wide-field Infrared Survey Explorer (WISE) (Cutri et al. 2012). To avoid contamination from multiple sources, we used a search radius of 3″ and selected the closest sources to the observed coordinates. Crossmatching with 2MASS and using a quality cut of "AAA" reduced the sample size to 45,376. This sample was then crossmatched with Gaia Data Release 3 (DR3) to obtain astrometry and optical photometry, which further reduced the sample to 45,268. The sample further reduced to 44,520 sources upon crossmatching with the WISE catalog. Of this, we considered only 43,329 LELS with distance values available from Bailer-Jones et al. (2021). The line-of-sight extinction values for our sample were obtained using the probabilistic galactic dustmaps model, Bayestar 2019 (Green 2018).

3. Late-type Emission-line Stars: Classes and Classification Schemes

In this section, we provide an overview of LELS along with its literature and the classification criteria employed in segregating them into different classes.

3.1. Classes of LELS

We categorize LELS into four classes:

1. IR excess sources
2. PtMS sources
3. Fe/Ge/Ke sources
4. dMe sources

IR excess sources are characterized by the presence of circumstellar disks or envelopes composed of dust and gas. These structures absorb stellar radiation and subsequently emit it at longer wavelengths, resulting in an excess of IR radiation in their spectral energy distribution (SED). Accretion disks are commonly found around YSOs, such as protostars, T Tauri stars (TTSs), and Herbig Ae/Be stars (Groenewegen 2012; Hartmann et al. 2016; Brittain et al. 2023). Some evolved stars, including those classified as asymptotic giant branch (AGB) stars and red giants, also exhibit IR excess (Groenewegen 2012). The accretion disk and mass loss are the major reasons for the formation of emission lines in these objects (Muzerolle et al. 1998a).

PtMS stars, ranging in spectral types from F0 to M9, represent stars that have transitioned beyond their main-sequence phase, generally classified into red giant branch (RGB) stars, horizontal branch (HB) stars, and AGB stars, based on their evolutionary phase. Activity in these sources is due to phenomena such as stellar winds, mass ejections, and pulsations. One of the well-studied groups of PtMS is the Mira variables, where activity happens in the form of long, periodic pulsations (Wood 1979; Yao et al. 2017). In stars such as RGBs and K supergiants, variability in Hα has been observed, which has been directly correlated with the mass loss (Vasu Mallik 1982; Cacciari & Freeman 1983).

dMe stars exhibit significant magnetic field due to the presence of convective outer layers and rapid rotation (Hall 2008). The magnetic fields are generated by dynamo processes, where the convective material is moved within the star's convective zone, which amplifies the magnetic field. These will lead to starspots, flares, and prominences in low-mass sources. Metallic lines such as Fe, Ca, and Na, which are sensitive to magnetic field, can be utilized to study magnetic field effects such as Zeeman splitting and Stokes broadening (Morin 2012). Higher resolution spectra of these sources will help accurately study the effect of magnetic field in these sources. Red dwarf emission stars (dMe stars) exhibit emission in Hα and/or Ca II H and K, both of which serve as indicators of chromospheric activity. dMe stars were classified into weak dMe stars ($0.1\ \text{Å} \leqslant \text{EW}(\text{H}\alpha) \leqslant 0.5\ \text{Å}$) and strong dMe stars ($\text{EW}(\text{H}\alpha) < 0\ \text{Å}$) (Kogure & Leung 2010). Furthermore, Joy & Abt (1974) classified dMe stars from dMs photometrically, compiling statistics on the frequency of occurrence of emission in Hα across different classes of M stars for the 426 M-type stars they observed. A spectroscopic investigation of the chromospheric activities on dMe stars was conducted (Cram 1989; Robinson et al. 1990), whereby the intensity and excess emission in a few of the observed emission lines were modeled (Young et al. 1989). Studies on activity indices of dMe stars along with their relationship with age were also carried out (Vaughan & Preston 1980; Pace et al. 2009). There is a special class of dMe stars known as flare stars or UV Ceti

type stars, which show emission in Hα, Ca II H and K, and in some cases, He and Na in emission during their quiescent state. Most of these lines get enhanced during flare state (Eason et al. 1992). Flares in M dwarfs are explosive events that occur as a result of magnetic reconnection in the atmosphere. A sample of 49 M dwarfs was studied for different spectra observed over a period of time using SDSS (Hilton et al. 2010). Further, 49 more flaring M dwarfs were detected using GALEX data by Welsh et al. (2007). The far-ultraviolet (far-UV) activity of the M-dwarfs was studied by France et al. (2018). Flares in 480 M dwarfs were identified, and Martínez et al. (2020) created a catalog. The LAMOST survey offers supplementary spectral information for M-type stars. This information comprises the EWs and errors of Hα as well as the spectral indices of other molecular bands, including CaH and TiO_5. The line strengths of TiO versus CaH are used as a popular method in the separation of late-type giants from dwarfs (Mould & Wallis 1977; Zhong et al. 2015; Yi et al. 2019). The CaH molecular band acts as an indicator of surface gravity, whereas TiO acts as a temperature indicator.

Fe/Ge/Ke sources are F-, G-, and K-type main-sequence stars or dwarfs, respectively, showing a considerable amount of chromospheric activity leading to the formation of the emission of lines such as Hα and Ca II H and K. In the Sun, non-radiative heating is closely linked to the magnetic field, which drives chromospheric activities such as sunspots and flares, ultimately resulting in the emission of Ca II (Robinson et al. 1990). Young stars such as weak-lined TTSs will also be included in this group due to the absence of IR excess (Gras-Velázquez & Ray 2005; Padgett et al. 2006).

3.2. Classification Criteria

In this section, we elaborate on the classification criteria employed for the separation of LAMOST LELS into different categories.

3.2.1. Identifying Sources with Infrared Excess

We made use of the 2MASS-WISE color–color diagram (CCDm) for separating young stars showing IR excess. Generally, YSOs are classified into Class I, Class II and Class III sources based on the continuum slope in the IR region of the SED of the star (Lada 1987). Class I sources are protostellar candidates that are deeply embedded in the molecular clouds, and Class II sources are classified as TTSs that have almost dispersed their envelope, but still have an accretion disk around it (Andre et al. 1993). Class III sources are evolved YSOs where disk dissipation is underway. Koenig & Leisawitz (2014) introduced the criteria to classify the YSOs into various classes using the 2MASS-WISE CCDm. In Figure 1(a), we have reproduced the YSO classification using the criteria mentioned in Koenig & Leisawitz (2014) which is listed below.

For Class II sources,

$$\begin{array}{l} H - K_s > 0 \\ \text{and} \\ H - K_s > -1.76^*(\mathrm{W_1} - \mathrm{W_2}) + 0.9 \\ \text{and} \\ H - K_s < (0.55/0.16)^*(\mathrm{W_1} - \mathrm{W_2}) - 0.85 \\ \text{and} \\ \mathrm{W_1} \leqslant 13 \end{array},$$

and for Class I sources,

$$H - K_s > -1.76^*(\mathrm{W_1} - \mathrm{W_2}) + 2.55.$$

Given that the primary focus of this section is to segregate young sources, we utilized the LAMOST spectral type classification. Consequently, stars identified as giant-M-type ("gM") by LAMOST were removed from the sample. This step effectively reduces the contamination of evolved stars in our data set.

After applying this additional criterion, we segregated a sample of 438 IR excess sources.

3.2.2. Identifying PtMS ELS Candidates Based on log(g) and CMD Estimates

To segregate PtMS sources from our sample, we employed a series of three systematic steps, drawing upon the remaining sample of 42,891 sources. As a first step, we separated PtMS candidates using the available surface gravity ($\log(g)$) value from LAMOST. We segregated sources based on the criterion that the value of $\log(g)$ exceeded three times its associated error (σ). Specifically, we applied the commonly used threshold of $\log(g) \leqslant 3.5$, which is typically employed to distinguish between giants and dwarfs (Batalha et al. 2010; Singh et al. 2019). Applying the above criteria to the remaining sample, we classified 2293 sources as PtMS candidates.

In addition, for M-type stars, the LAMOST pipeline classified their spectral types as dwarf M (dM)-type stars and giant M (gM)-type stars. In our remaining sample, 49 more sources belong to the gM type, which makes the new sample 2342 PtMS candidates.

For the 7618 sources lacking LAMOST $\log(g)$ values, color–magnitude diagram (CMD) was employed to identify PtMS candidates within that sample. Ruiz-Dern et al. (2018) used Gaia-2MASS CMD to segregate red giant candidates in their sample. The availability of a larger sample and the presence of other predefined cuts to distinguish PtMS sources helped us retool the CMD cut to separate PtMS sources in our sample. For this purpose, we utilized Gaia CMD.

The criterion we defined to segregate our data is mentioned below

$$\begin{array}{l} M_G < 4.35 \\ G_{\mathrm{BP}} - G_{\mathrm{RP}} > 1 \\ M_G < 3.875(G_{\mathrm{BP}} - G_{\mathrm{RP}}) - 1.3 \end{array}.$$

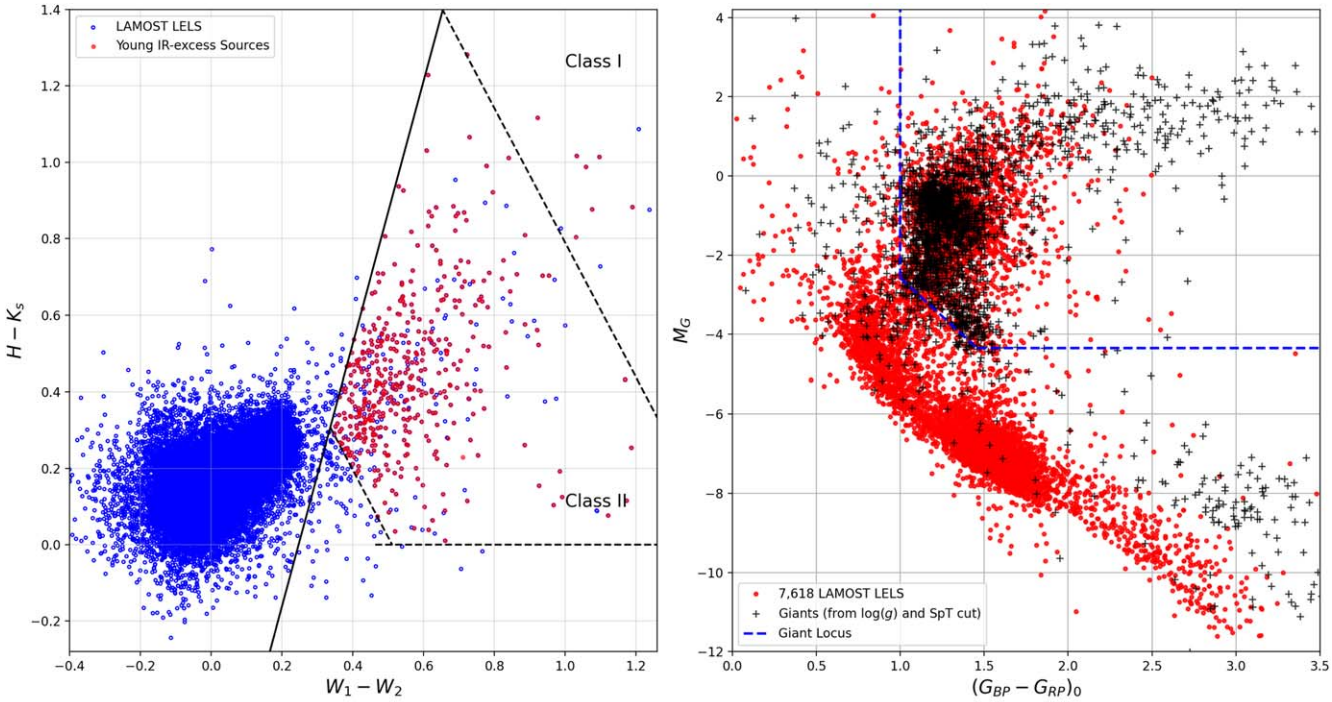

Figure 1. (a) The 2MASS-WISE CCDm for the selection of young IR-excess candidates from LAMOST DR6 is displayed in the left panel. The blue dots represent the entire sample of LELS, and the red dots represent IR-excess sources. The dashed and solid lines represent the selection region for Class I and Class II sources defined in Koenig & Leisawitz (2014) respectively. The blue dots in the Class II region represent stars with spectral types "gM." (b) Gaia CMD for the selection of LAMOST PtMS candidates is displayed in the right panel. The red dots in the plot represent 7618 LAMOST LELS, whose selection is mentioned in Section 3.2.2. The black crosses represent PtMS candidates segregated using the log(g) and the spectral type (SpT) cuts. The blue dashed line represents the region dominated by PtMS candidates.

The Gaia CMD of the LAMOST PtMS candidates is shown in Figure 1(b). Applying the above mentioned criteria of magnitudes and colors we included an additional number of 2327 sources in our sample. Combining all three samples obtained using the above criteria, we obtained a final sample of 4669 PtMS candidates.

3.2.3. Fe/Ge/Ke/dMe LELS Candidates

From the rest of the sample (38,222 sources), sources exhibiting [N II] and [S II] in emission are separated and categorized as "forbidden-line sources," totaling 5177 sources. These stars will be further discussed in B. Shridharan et al. (2024, under preparation). The remaining sample was classified into Fe/Ge/Ke stars and dMe stars based on their spectral types provided by LDR6. Since the LAMOST spectral type has been used as a classification scheme, validation of the spectral type for LELS sources is necessary. Hence, we plotted a comparison of the LAMOST spectral type with the Gaia spectral type of our sources, as shown in Figure 2. The Gaia spectral types are estimated using General Stellar Parametriser (GSP) modules (Vallenari et al. 2023). The figure shows that other than G-type stars, all the other spectral types provided by LAMOST are fairly accurate.

Furthermore, the reason behind the separation of dMe stars from other LELS is the presence of intense molecular bands in M-type stars. None of these stars show IR excess. Hence, this sample contains a mix of potential class III sources, active main-sequence LELS, and different types of variable stars. Further studies on young stars in this class are conducted by Nidhi et al. (2023). Figure 3 illustrates the flowchart of the entire classification scheme.

4. Results

In this section, we discuss the distribution of LELS in the galaxy and the classification based on the major spectral features.

4.1. Distribution of LELS Across the Spectral Range

Summarizing the classified sample, we have a data set of 438 IR excess sources spanning spectral types F6-M7, 4669 PtMS sources across spectral types F0-M9, 9781 Fe/Ge/Ke sources, and 23,264 dMe sources. This summary is tabulated in Table 1.

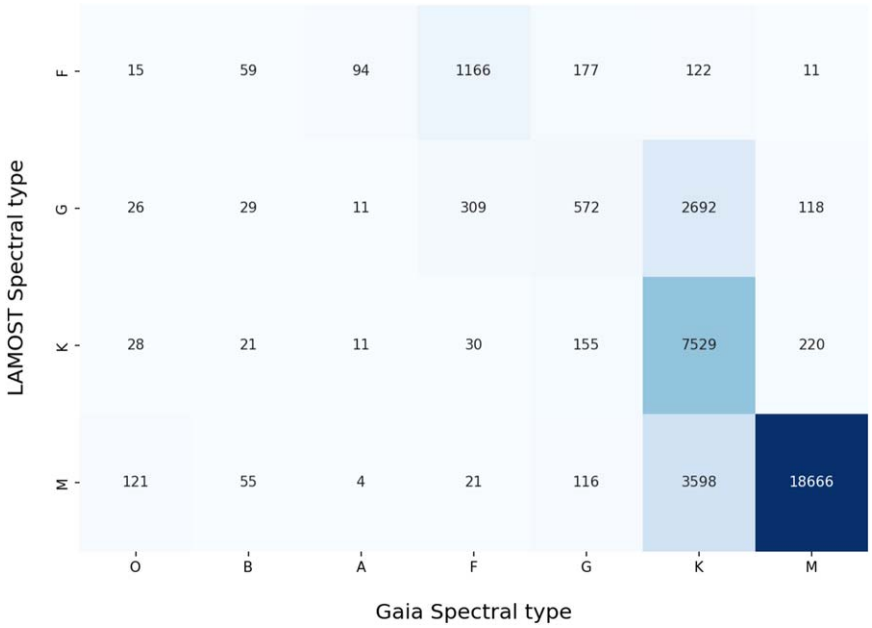

Figure 2. The number distribution plot of the LAMOST spectral types vs. Gaia spectral types of our sample of LELS.

Furthermore, the distribution of LELS over the entire late-type spectral range is depicted in Figure 4. From our sample of 38,152 LELS, we observed that the number of ELS increases between the spectral range of K5 to M5. When comparing with the total number of observed sources in LAMOST, this increase in number of ELS is very significant. This shows a direct correlation of higher activity in well-developed chromospheres. The number of stars steeply decreases after M6. The ELS that are observed after M5 are predominantly PtMS candidates. We conducted a crossmatch with SIMBAD to identify sources previously studied in the literature. This analysis revealed that 8643 sources had already been documented, resulting in a newly detected sample of 29,509 LELS. A detailed description of the known sample of each class of LELS will be provided in Section 4.6.

4.2. 3D Distribution of LELS in the Galaxy

Employing the methodology mentioned in Section 3.2, we have compiled a sample of 38,152 LAMOST LELS. We have obtained the distances from Bailer-Jones et al. (2021). Figure 5 shows the galactocentric distribution of LELS present in our sample, where $(-8000\,\mathrm{pc},\ 0\,\mathrm{pc})$ of $(X,\ Y)$ represents the position of the Sun. Around 81% (30,145) of 38,152 LAMOST LELS are at a distance less than 1 kpc. Among them, 22,862 are dMe stars, which constitute over 98% of the entire dMe sample spread over all the distances. More than 77% (6628) of the 9781 Fe/Ge/Ke stars are observed within 1 kpc, and another 18% (1555) of them are observed between 1 and 2 kpc. In the case of IR excess sources, 320 out of 438 of these sources are observed within a distance of 1 kpc. The major contrast is observed in the case of PtMS candidates. Only 7% (335) of 4669 PtMS candidates are observed at a distance within 1 kpc. Over 72% (3343) are observed between 1 and 5 kpc. Similar to the spatial distribution observed in Shridharan et al. (2021), the majority of LELS data is also distributed along the galactic anti-center direction.

4.3. Photometry of LELS

We utilized photometric data provided by 2MASS and Gaia to further study the distribution of our LELS data set. Figure 6 shows the kernel density estimate (KDE) photometric distribution of our LELS sample. It also helps us to validate the classification schemes utilized for our sample. The CMD of our LELS sources is represented in the left panel of Figure 6. The zero-age main sequence (ZAMS) line is also shown in the figure. The IR excess source distribution (represented in red) is located in the region above the ZAMS line, whereas Fe/Ge/Ke sources (represented in yellow) and dMe sources (represented in blue) are over-plotted on the ZAMS line. The PtMS sources (represented in green) highlight the sub-giant, AGB, and RGB regions of the Hertzsprung–Russell (HR) diagram (Eyer et al. 2019).

The CCDm of the LELS is shown in the right panel of Figure 6. We used the same color scheme for the CCDm as described for the CMD. It has been observed that the majority of the IR excess sources are located around the TTS locus (Meyer et al. 1997), as shown in the figure. We also notice that the PtMS sources from our sample are clustered around the

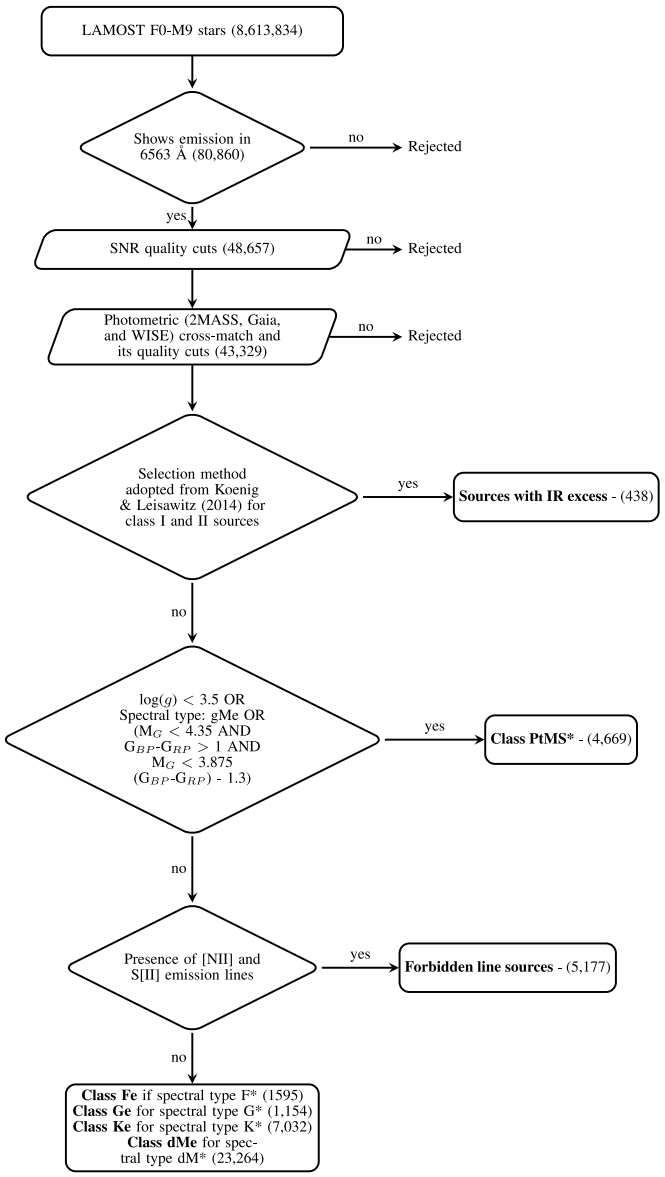

Figure 3. Flowchart of the classification criteria of LELS.

"giant locus" (Carpenter 2001). The rest of the sample is clustered around the main sequence line. These distributions bring novelty to our classification scheme and bring validity to our sample.

4.4. Spectral Features of LELS

In this section, we mention the major emission lines observed in late-type stars. The major features include Balmer lines, metallic lines like Ca II H and K, CaIRT, Mg, and Na doublet, and molecular bands such as TiO and VO for stars of spectral types later than K5. Figure 7 shows the representative spectrum of a sample IR excess source.

Table 1
Statistics of Different Classes of LAMOST LELS in Our Study

Type	ELS Candidates
Total late-type stars	8,613,834
Stars with Hα	80,860
After 2MASS, Gaia, WISE crossmatch	43,329
Young IR excess Sources	438
PtMS Candidates	4669
Forbidden line sources	5177
Fe/Ge/Ke Candidates	9781
dMe Candidates	23,264

As we discussed in the previous sections, all the LAMOST LELS star spectra show Hα in emission. The strength of this line is indicative of the circumstellar activity of the star or the stellar system. Other Balmer lines like Hβ, Hγ, and Hδ are also observed in a number of the LELS. The statistics of these observations, along with the line strength measurements, are studied.

Other major emission lines observed include the Ca II H and K lines, which are observed either in emission or absorption. These lines, along with Balmer lines, are presented in the literature as chromospheric activity tracers. Another significant ionized calcium line observed in LELS is the CaIRT (λ8498, 8542, 8662 Å). Except for a number of IR excess sources, very few stars show triplet emission in their spectra.

Given their late-type classification, it is common to observe metallic lines in the spectra of these stars. The main metallic lines include Na I doublets at 5890, 5896 Å, Na I (λ 8183, 8195 Å), Mg I (λ 5184 Å), K I (λ 7665, 7701 Å), Fe I (λ 4383, 5270 Å), Ca I (λ 4226 Å), etc. These lines are often observed in absorption. A few other metallic lines like Fe II (λ 5018, 5168 Å), Fe I (λ 4063, 5162 Å), and the forbidden line of [O I] (λ 6300 Å) are also observed in emission. Figure 8 displays representative spectra from the Fe, Ge, Ke, and dMe classes.

The major molecular bands observed in late-type stars include TiO (band heads at λ 4760, 5160, 7050, and 7580 Å), which are prime indicators of the temperature of a star. These bands dominate the spectra of late-K to M-type stars. Other major molecular bands observed include VO (band heads at λ 7010, 7383 Å) and CaH (band heads at λ 6400, 6800 Å).

The emission line profile of our sources shows various types of line features. The intensity of emission varies depending on the level of activity in these sources. The mass column density of the chromospheres and temperature structures inside the chromosphere will significantly affect the line profiles and line intensity of low mass sources (Houdebine et al. 1995). The literature shows that most of the profiles can be attributed to the inclination angle, stellar rotation, or chromospheric activity of these sources. Furthermore, strong asymmetry in emission profiles has been observed in red giants and long period variables (LPVs) (Gillet 1988). Given the large sample

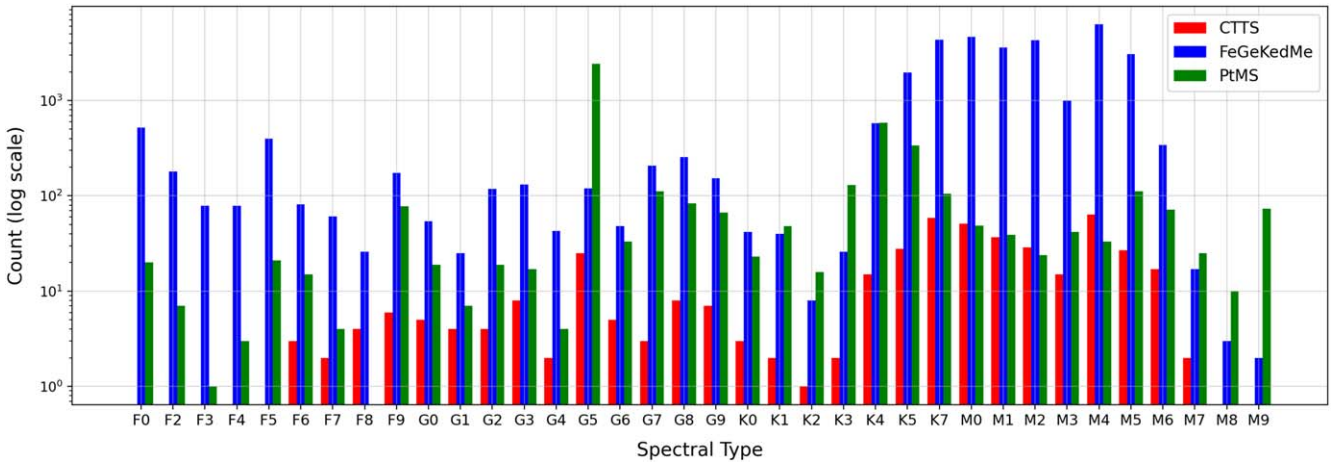

Figure 4. Histogram of LELS from LDR6. The spectral type is marked on the diagram along with different classes of LELS. The counts of stars belonging to each spectral type are represented in log scale.

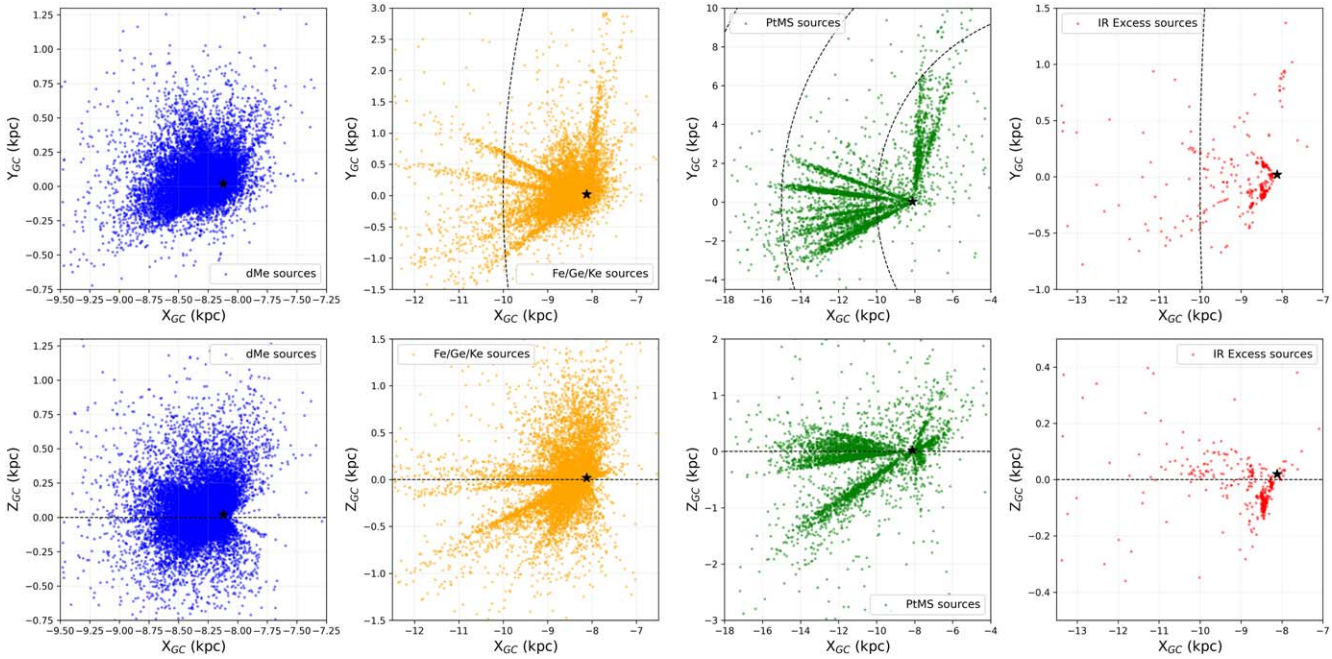

Figure 5. A galactocentric distribution of LELS sources from LAMOST DR6. This coordinate system places the center of our galaxy as the origin and (X_{GC}, Y_{GC}, and Z_{GC}) are the Cartesian coordinates. The Galactocentric X_{GC} (in kpc) vs. Galactocentric Y_{GC} (in kpc) is plotted in the upper panel and Galactocentric X_{GC} (in kpc) vs. Galactocentric Z_{GC} (in kpc) is plotted in the lower panel. The majority of the sources are observed in the anti-center direction. The LAMOST dMe stars (blue), PtMS candidates (green), Fe/Ge/Ke stars (orange), and IR excess source (red) candidates are represented in this plot. The asterisk in all the plots shows the position of Sun. The dotted line on the upper panel represents the galactic rings, representing distances of 10 kpc and 15 kpc from the galactic center. The dotted line on the lower panel represents galactic disk ($Z_{GC} = 0$) plane.

size of nearly 40,000 LELS, classifying the line profile of each source presents a significant challenge and falls outside the scope of this catalog. This detailed classification will be reserved for future studies, where individual groups of LELS will be analyzed in greater depth (Anusha et al. 2021; Nidhi et al. 2023).

In our work, we have estimated the EW of major lines like Balmer lines (Hα, Hβ, Hγ, and Hδ), Ca II H and K, and CaIRT using the `line_index` module of the `laspec` package by implementing an automated Python routine. This module gives us the values of EW and EW error for all the respective lines. Within our study, a value for the emission-line EW is deemed

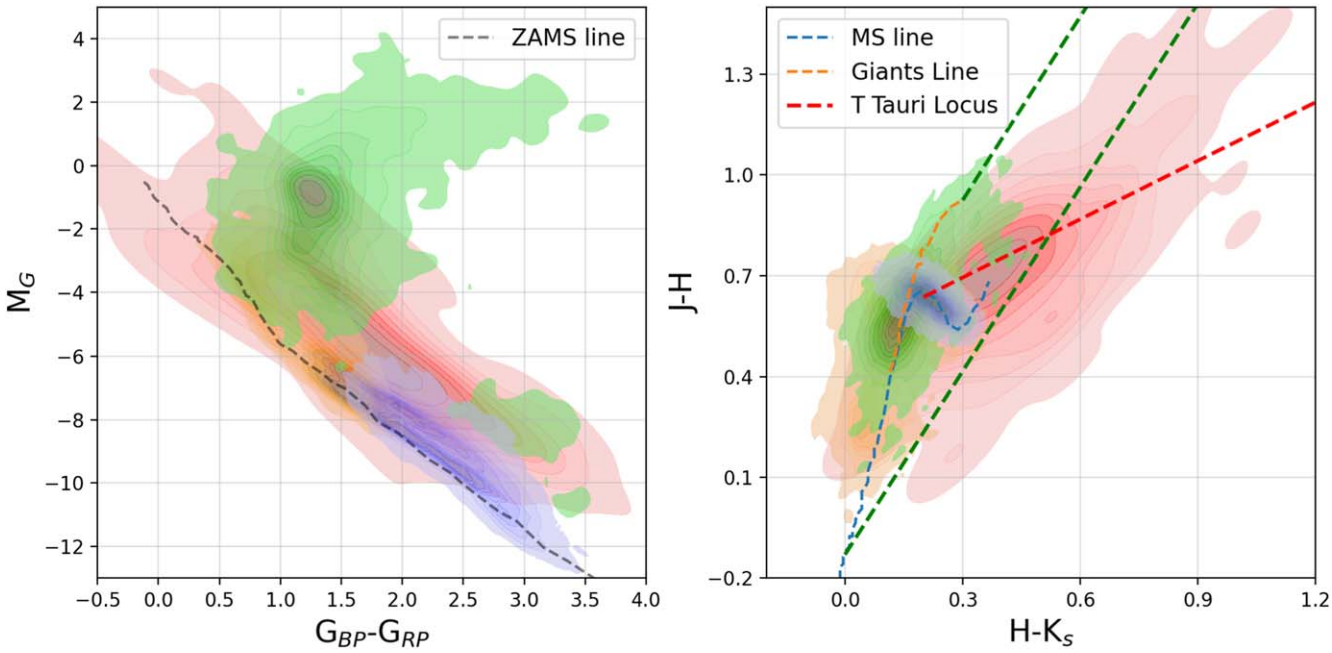

Figure 6. The KDE distribution of Gaia CMD (left) and 2MASS CCDm (right) of LAMOST LELS. The extinction correction of all the magnitudes has been done using the Bayestar dust map (Green 2018). Both the plots feature dMe stars (blue distribution), Fe/Ge/Ke sources (yellow distribution), PtMS candidates (green distribution), and IR excess sources (red distribution). Also, the ZAMS line (black dashed line), main-sequence loci (blue dashed line), giants line (orange dashed line), and TTS locus (red dashed line) are also shown (Carpenter 2001).

legitimate only if the matching EW value is three times the projected error (σ) supplied by *laspec* (EW $> 3\sigma$).

4.4.1. Balmer Lines

Hα in emission is one of the major indicators of activity in low-mass stars. In sources with IR excess, predominantly in young stars, the emission arises from the magnetospheric columns (Hartmann et al. 1994), giving rise to very intense emission lines. From the literature, a significant correlation between stellar rotation and magnetic activity has been observed in low mass stars. Studies that have compared star rotation to activity characteristics have found that the relationship is valid for sources that are fully or partially convective (Delfosse et al. 1998; Reiners et al. 2012). Rotation rates will also play a major factor. A clear association has also been found between stellar rotation and EW(Hα) (Newton et al. 2017).

Figure 9 represents the histogram of EW of Hα in various classes of LELS. The bin size for the histogram is calculated using the Freedman–Draconis rule (FDR) for each sample. For those with bin sizes estimated to be too small using the FDR method, the bin sizes are provided manually. This is the rule followed throughout this work for histogram distributions.

Figure 9(a) presents the histogram distribution in the Hα strength (EW(Hα)) for IR excess sources. Observations indicate that IR excess sources exhibit the most intense Balmer emissions compared to other classes. They have a median value of -19 Å, as the strength is primarily due to disk accretion, as mentioned earlier. Figure 9(b) shows the emission histogram distribution for PtMS sources, and it shows a median value of -4 Å. The strength of the line is minimum for dMe candidates (Figure 9(d)) with a median value of -3.2 Å. The models of Hα emission in TTS suggest that the emission strength can vary due to rotation, turbulence, and non-axisymmetric accretion in these sources (Kurosawa et al. 2005; Wilson et al. 2022). Stellar winds are also one of the causes, which account for the increased line strength in CTTSs (Lima et al. 2010). In the case of main-sequence late-type stars, the presence of Hα emission is attributed to chromospheric and coronal activity. In solar-type sources, all active phenomena are directly correlated with the presence of intense magnetic fields generated by a dynamo mechanism (Charbonneau 2014).

A total of 27,642 LELS show emission in Hβ. They include 341 IR excess sources, 2779 PtMS candidates, 3703 Fe/Ge/Ke stars, and 20,819 dMe candidates. Over 86% of IR excess sources and more than 85% of dMe candidates show emission in Hβ. Only 35% of PtMS candidates and 50% of Fe/Ge/Ke candidates show Hβ emission. The strength of emission ranges from -0.84 to -100 Å, with a median value of -2 Å.

4.4.2. Ca II Emission Lines

Ca II emission lines are observed in late-type stars, both in the bluer and redder ends of the spectra. We observed Ca II H

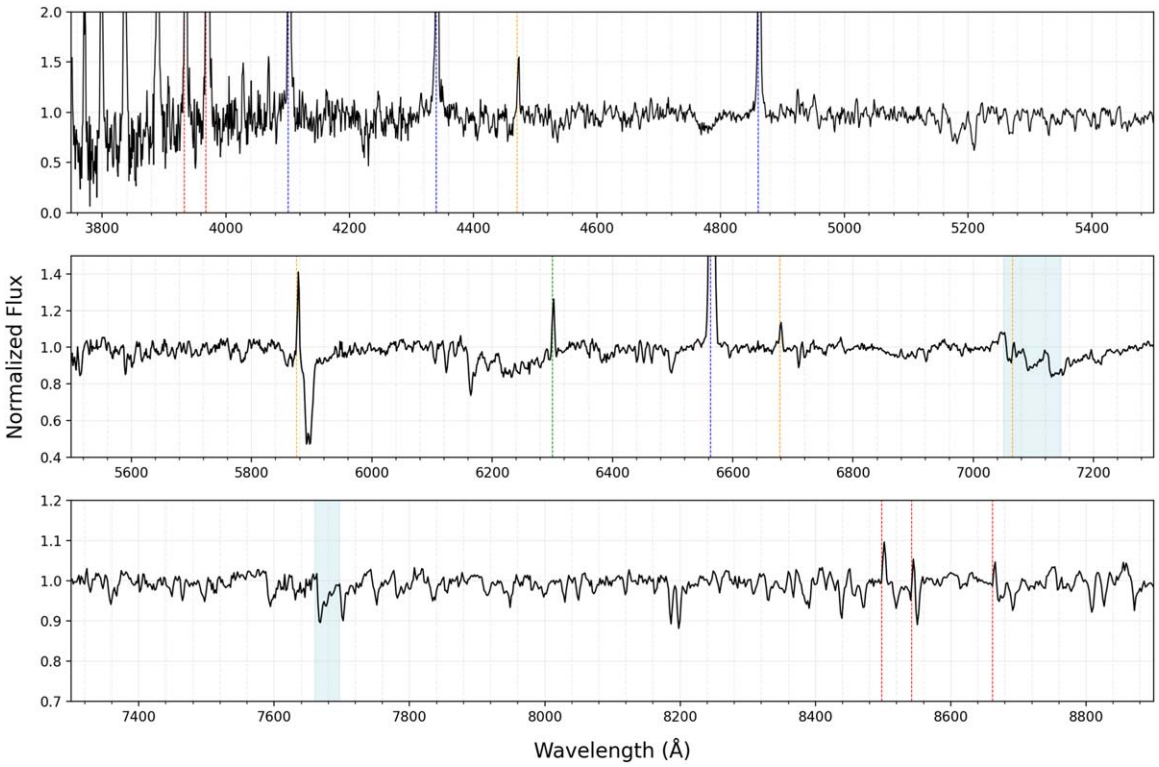

Figure 7. Visualization of the representative spectrum of a LAMOST TTS. The Balmer lines are represented in blue, Ca II lines in red, [O I] in green, and He I lines in orange. Furthermore, TiO bands are highlighted in blue. The spectra belong to the star IQ Tau, a TTS of spectral type M2.

and K lines at wavelengths 3968 Å and 3933 Å, respectively and the CaIRT are observed at wavelengths 8498, 8542, and 8662 Å. Mould & Wallis (1977) studied these emission lines and their dependencies with luminosity and precisions on other physical attributes in these objects.

From our sample, it has been observed that 4887 LELS show emission in Ca II H, among which 164 (37%) are IR excess sources, 141 (3%) are PtMS candidates, 722 (8%) are Fe/Ge/Ke stars, and 3860 (17%) are dMe stars. The presence of emission/absorption contribution from the H I line in Ca II H suggests the necessity of distinguishing between the contributions of both for subsequent analyses. This separation is crucial for future investigations.

Here, 6215 LELS show emission in Ca II K, with EW values in the range −2.5 to −55 Å. Around 39% of IR excess sources (170), more than 18% of dMe stars (4315), over 3% of PtMS sources (155), and close to 18% of Fe/Ge/Ke sources (1575) show emission in the Ca II K line. This emission line is prominently observed in M-type stars, i.e., stars having effective temperatures of $T_{\rm eff} < 4000$ K. This holds in the cases of young IR excess sources as well. Figure 10 displays the histogram distribution of EW (Ca II K) for various classes of LELS.

From the estimation of line parameters, it has been observed that the CaIRT in emission is seen rarely in main-sequence late-type stars. Here, 893 stars show emission in the Ca II 8498 Å. More than 50% of the IR excess sources (212), 505 dMe stars, and 86 PtMS candidates show emission in Ca II 8498 Å. The range of emission of Ca II 8498 is from −0.4 to −17 Å. The other two lines of the CaIRT show a similar EW distribution. Ca II 8542 emission is seen in 310 stars, of which 176 are IR excess sources, 62 are dMe stars, and 37 are PtMS candidates. For the Ca II 8498 Å emission line, over 40% of IR excess sources show emission in this line, with EWs ranging from −0.4 to −58 Å; 323 stars show emission in the Ca II 8662 Å emission; 178 IR excess sources and 50 PtMS candidates show emission in Ca II 8662 Å; 232 of the 38,152 LELS show emission in all lines of the CaIRT; 166 IR excess sources, 12 Fe/Ge/Ke stars, 28 dMe stars, and 26 PtMS candidates show emissions in all three lines.

The majority of the stars that show emission in these sets are IR excess sources. This confirms that the presence of CaIRT emission indicates the youth of these objects as well. Most of the IR excess sources belong to the class of TTSs and the stellar properties and mass accretion rates of these stars are studied in Nidhi et al. (2023).

4.4.3. Paschen Lines

Paschen lines were also seen in the emission of some LELS. The EWs of P12, P14, and P17 are calculated initially since

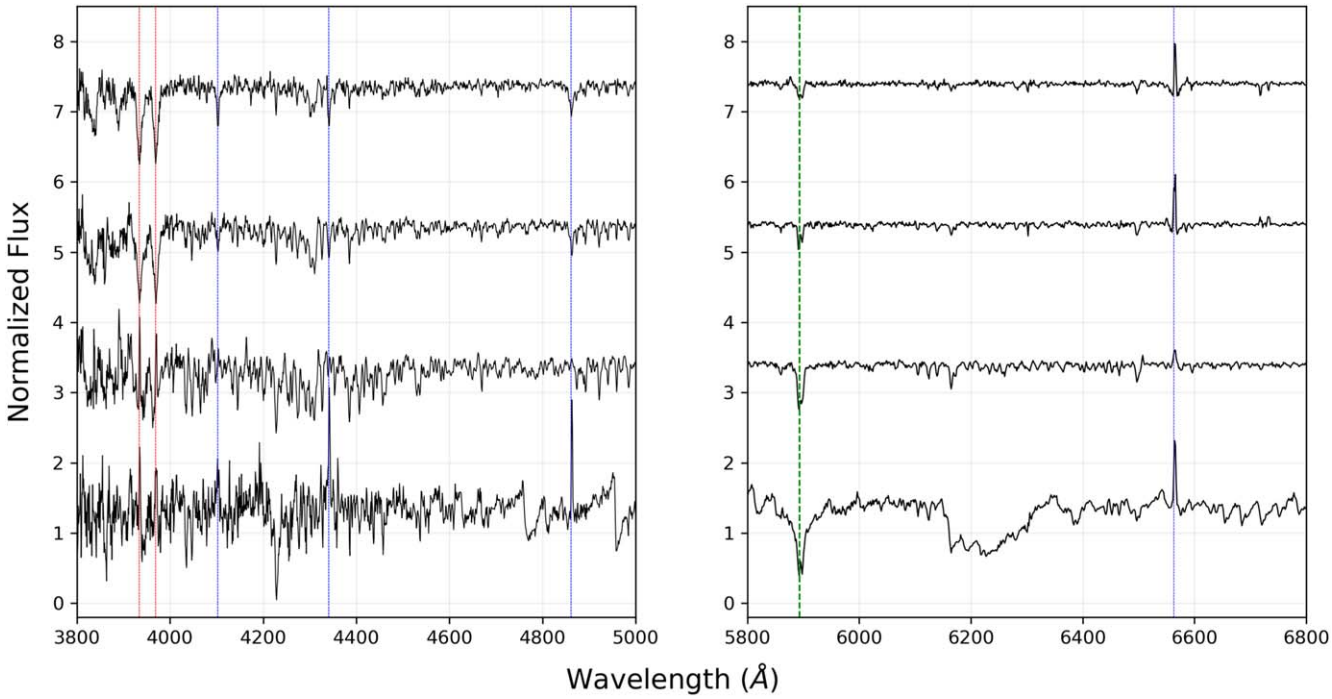

Figure 8. The representative spectra of a sample LAMOST Fe/Ge/Ke/Me candidate. The Balmer lines are represented in blue, the Ca II H and K lines are represented in red, and Na I doublet in green. The spectral types of each of these individual spectra are also represented.

these lines do not overlap with the Ca II triplet; 916 LELS showed emissions in P12. The emission is seen in the range of −0.2 to −1.25. The line is mostly seen in Fe/Ge/Ke stars, as 422 of them show emission in P12, which includes 16 IR excess sources, 180 PtMS candidates, and 253 dMe stars. The P14 line is seen in emission in 641 LELS; 242 Fe/Ge/Ke stars, 236 dMe stars, 98 PtMS candidates, and 12 IR excess sources show emissions ranging from −0.2 to −1.4; 1762 stars show emissions in the P17 line; 948 dMe stars, 597 Fe/Ge/Ke stars, 210 PtMS candidates, and 17 IR excess sources show P17 emission. Paschen emission is not common in IR excess sources, whereas Ca II triplet is seen more often.

4.5. Relation Between Spectral Type and Major Emission Lines

Figure 11(a) shows the variation of the Hα EW with respect to the spectral type for IR excess sources, PtMS candidates, and Fe/Ge/Ke/dMe stars. Also, Hβ displays a similar distribution over the late-type spectral range in emission as that of Hα, as shown in Figure 11(b). The strength of emission from these sources peaks toward the later K- to M-type sources. Studying this allows for a deeper understanding of the emission trends across the spectral range and facilitates the comparison of the presence or absence of various emission lines. This, in turn, aids in elucidating the emission mechanisms in these sources.

Ca II K is one of the most active chromospheric indicators (Hall 2008). Figure 11(c) depicts the emission strength of Ca II K over various spectral types. The notable thing is the presence of emission of Ca II K in LELS sources of spectral types later than K5. This is because of the presence of chromospheric activity in those sources. Among the stars in the spectral range F6–K4, less than 1% of them show emission in Ca II K, while more than 40% of sources later than K4 show emission. This suggests the presence of active chromospheres and coronae in sources with spectral types later than K5 (Young & Koniges 1977; Hall 2008).

4.6. Literature Crossmatch of known LELS

The SIMBAD crossmatch of these objects provided us with a sample of 373 stars from a total of 438 IR excess sources. Of the 373 known stars, 317 belong to four main classes. They are TTau*/TTau candidates, YSOs/YSO candidates, Orion V*, and Em* classes. Also, the classes "Star" and V* contribute to 24 more candidates. These contribute to 94% of the known sample. Our sample has 65 newly detected IR excess sources.

The evolved stars are separated from other classes based on the method mentioned in Section 3.2.2. It provided us with a sample of 4669 PtMS candidates. The SIMBAD crossmatch has provided us with a known sample of 944 stars. From that crossmatched sample, we observe that 160 stars belong to different PtMS star classes, which are asymptotic-giant branch

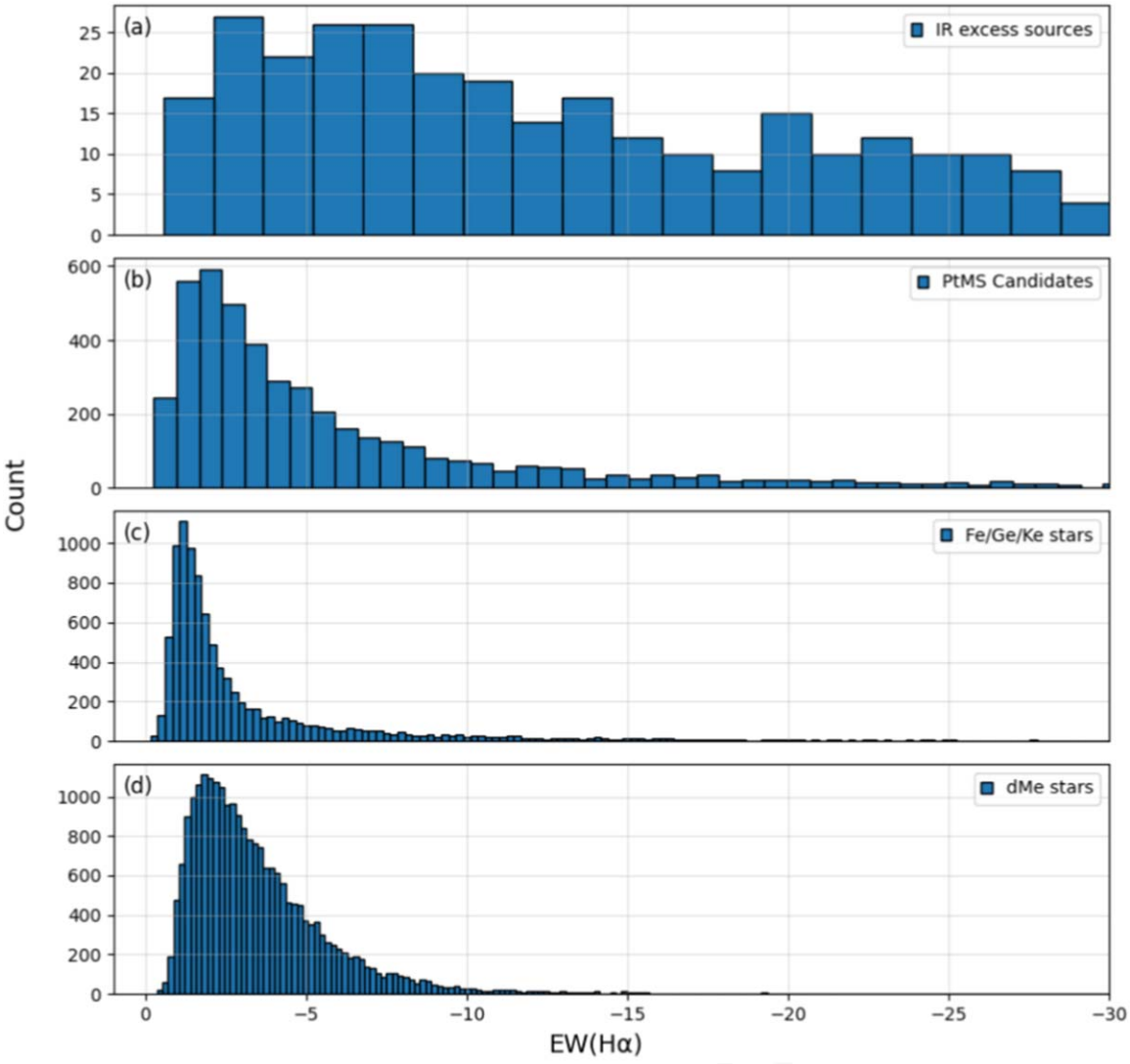

Figure 9. The figure represents the histogram of EWs of Hα for various classes of LELS. The histogram contains IR excess sources, PtMS candidates, Fe/Ge/Ke stars, and dMe candidates.

stars (AGB*), horizontal branch star (HB*)/HB* candidates, Mira variables/Mira candidates, red-giant branch star (RGB*)/RGB candidates, red supergiants, and post-AGB* cases. Also, there are 88 long period variable star (LPV*)/LP* candidates; 81 of the known samples belong to binary classes like eclipsing binary stars (EB*) or EB* candidates, symbiotic stars (Sym*), spectroscopic binaries (SB*), and RS Canum Venaticorum (RS CVn) cases. Variable star classes like pulsating variables (Pul V*), eruptive variables (Eruptive*), variable stars (V*), ELS (Em*), Orion variables (Orion V*), BY Draconis variables (BY Dra), and pulsating variables (Pul V*) contribute to 150 more known stars; 115 stars are classified as YSOs as well. The presence of YSOs in this sample is evident from their location in the HR diagram and the lack of IR excess. These might be candidates of weak-line TTSs, which show an absence of IR excess and weak Hα emission (Alcalá et al. 1993). Also, 293 stars were represented in the "Star" class, and 14 were represented as low-mass stars (low-mass*). A couple of stars belong to groups such as Cepheids and far-infrared (FIR) sources, which sum up the known sample of PtMS stars. We have a sample of 3725 new detections, which do not have any information on SIMBAD.

A SIMBAD crossmatch of the dMe stars revealed that 5731 are previously detected stars, while 17,533 sources are new detections. Of the known sample, 1490 are categorized as "star/**" in SIMBAD; 1032 were mentioned as stars with higher proper motion (PM*); 1083 stars belong to various variable star groups like V*, Em*, Orion V*, and Eruptive*; 301

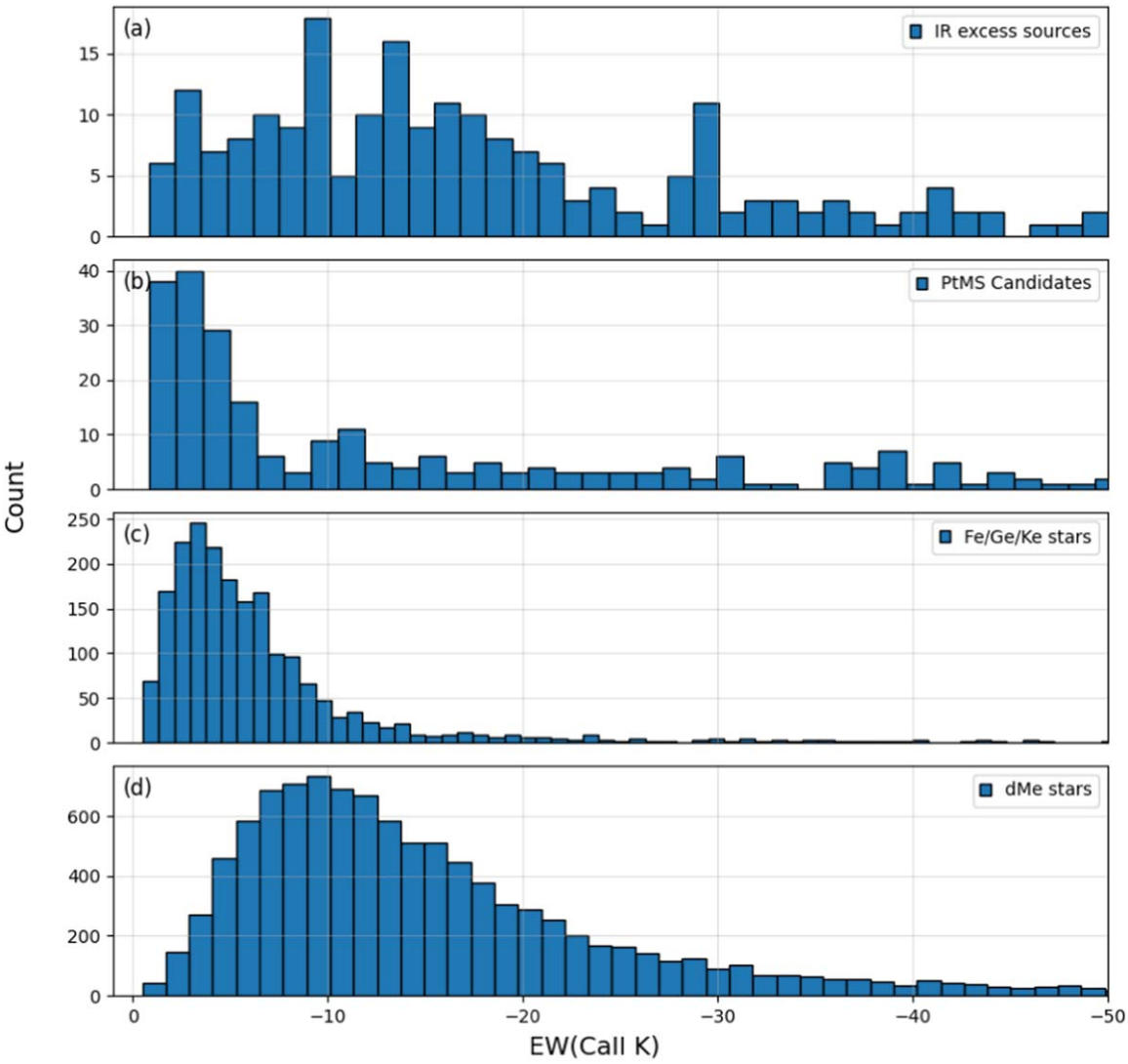

Figure 10. The distribution of EWs of major emission lines over the entire range of late spectral types of LAMOST LELS is displayed in the figure. Fe/Ge/Ke/dMe sources, PtMS candidates, and IR excess sources are shown in the plot.

belong to binary groups such as EB*, SB*, and RS CVns. This group also has 1322 YSO/YSO candidates. Other classes such as Pec*, mid-infrared (MIR), near-infrared (NIR), and radio sources also have a couple of stars each in every group.

From our sample of 9781 Fe/Ge/Ke stars, 1595 are Fe-type, 1154 are Ge-type, and 7210 are Ke-type. After the SIMBAD crossmatch of this sample, 1882 stars are determined as the known sample. Like other classifications, most of our known sample belongs to some variable star classes like Orion V*, V*, Em* (ELS), Eruptive*, PulsV*, and RotV*, which contribute to 484 stars; 531 of them are just represented as "stars," which can be converted to ELS after our LAMOST spectroscopic results; 281 are classified as young stars belonging to classes YSO/YSO candidates and Ttau*/Ttau* candidates; 315 of them are classified into binary star groups like EB*/EB* candidates and SB*. We have a sample of 7899 Fe/Ge/Ke sources as new detections. Our sample of Fe/Ge/Ke stars can be suitable candidates for further variability study to enrich the understanding of various active phenomena in these sources.

4.7. Classification of LELS Based on the Presence of Emission Lines

As mentioned in the previous sections, Hα, Ca II H and K, and CaIRT are the most commonly observed emission lines in LELS. The presence or absence of more than one of these emission lines will be of great physical significance. Hence, for our sample, we devised a classification scheme of LELS based on the presence or

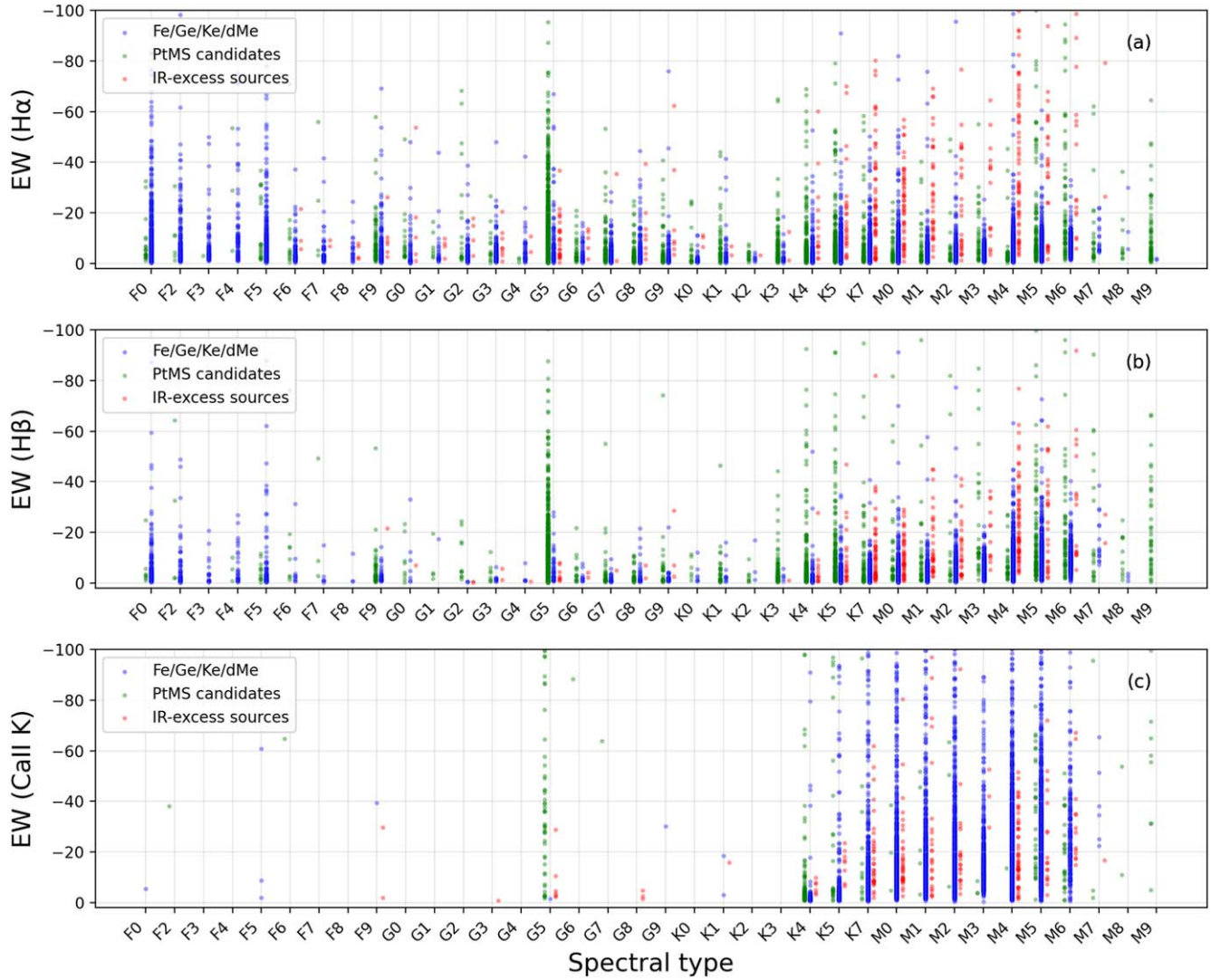

Figure 11. The distribution of EWs of major emission lines over the entire range of late spectral type of LAMOST LELS is shown in the figure. Fe/Ge/Ke/dMe sources (blue), PtMS candidates (green), and IR excess sources (red) are shown in the plot.

absence of three major emission lines, namely Hα, Ca II K (as a representative of Ca II H and K), and Ca II λ 8542 Å (the representative line from the Ca II triplet). Since we are using the entire range of spectra for this study, we had to consider some initial assumptions in terms of SNR at various spectral regions, especially in the u band. After visual inspection of the spectra, $SNR_u > 0.8$ was stated as the selection criterion for this study.

1. Group A comprises stars displaying emission in Hα, Ca II K, and CaIRT, totaling 142 stars. Intense emission lines are observed in this group, with a median Hα EW of −41 Å. More than 71% (101) of stars in this group belong to IR excess sources, 13.4% (19) belong to PtMS candidates, and 14% (20) belong to dMe sources. It was also noticed by Muzerolle et al. (1998b) that He I emission is also observed in these sources. We have observed that 93 sources show emission in He I λ 5876 Å in these sources. This is confirmed by the presence of weaker He I $\lambda\lambda$ 6678, 7605 Å emission lines. Moreover, the literature crossmatch revealed 66 stars classified as YSO/TTau stars and 47 categorized as Em*/OrionV* stars, indicating the majority of the sources belong to disk-like systems. This confirms the presence of young and active sources within this group. Figure 12(a) displays the KDE EW distribution of Hα, Ca II K, and CaIRT emission lines. This set is significant due to its implication on the line origin of emission of all three lines, indicating disk emission.
2. Stars that show emission in Hα and Ca II K are classified as Group B. This group contains 5898 stars, which include 66

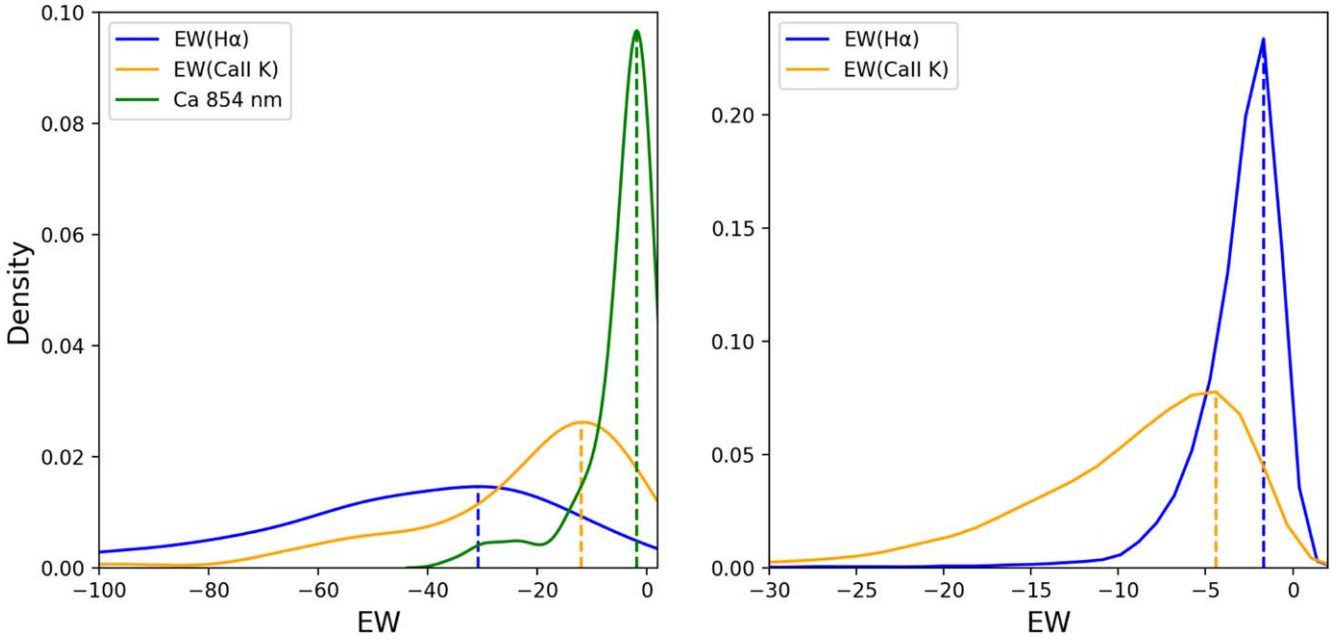

Figure 12. The KDE distribution of EWs of emission lines from Group A (left) and Group B (right). Hα is represented in blue, Ca II K in orange and Ca II 8542 Å in green. The corresponding dashed lines represent the number of stars showing the same EW.

IR excess sources, 133 PtMS candidates, 1548 Fe/Ge/Ke stars, and 4151 dMe stars. A noteworthy observation is that only ten stars, spanning all classes, have a spectral type less than K4. Also, we observed that 94% (5542) of sources exhibit a greater emission strength of Ca II K compared to Hα. Among the 2469 known stars within this group, 63% (1552) are classified under various variable star categories, including eruptive variables (Eruptive*), Orion variables, BY Draconis variables, etc., indicating the majority of sources show rotation coupled with starspots and other chromospheric activities. Figure 12(b) depicts the KDE distribution of the above mentioned lines. The strength of lines signifies that the lines originate primarily from the chromospheres in these sources. The strength difference in both these emission lines as mentioned above, also indicates the same scenario.

3. Group C contains stars that show emission in Hα and CaIRT; 25 stars belong to this group. It has been observed that the majority of the sample, along with the CaIRT, shows Paschen lines in emission. Of the 25 stars, nine are associated with IR excess sources, eight with Fe/Ge/Ke sources, two with PtMS sources, and six with dMe sources. Since the number of sources in group C is quite low, it suggests the probability of both Hα and CaIRT being in emission is minimal.
4. Group D contains stars that show emission in Hα alone. We have a sample of 3785 stars in this group. It contains 49 IR excess sources, 1164 PtMS candidates, 2057 Fe/Ge/Ke stars, and 515 dMe stars. A SIMBAD crossmatch of the known sample identified 1534 sources already studied in the literature. This group includes PtMS stars such as AGB*, RGB*, and Mira variables, as well as other variable star categories like Em*, V*, and OrionV*. This diversity indicates a wide range of activity among these sources, including mass loss, rotation, and chromospheric activity.

To conclude, the majority of sources in Group A belong to the IR excess source class. The line strength of major emission lines is also very intense for those sources. In Group B, the emission is predominantly due to chromospheric activity, suggested by the presence of a large number of sources belonging to Fe/Ge/Ke/dMe sources. It is also interesting to note the lack of sources earlier than K4 in this group, suggesting intense chromospheric activity in sources later than K4.

4.8. Catalog Description

The catalog of LAMOST LELS contains 38,152 sources, which include 438 IR excess sources, 4669 PtMS candidates, 9718 Fe/Ge/Ke sources, and 23,264 dMe sources. We further classified 9850 sources into four groups based on the presence or absence of Balmer and Ca emission lines, as described in Section 4.7. The sources are named with a common prefix of LM-LEMC (Low-Mass LAMOST EMmision-line Catalog) followed by the index. We have sources ranging from LM-LEMC_1 to LM-LEMC_38152. A sample table is shown in

Table A1. The data include the LAMOST design ID, positions, our classification and grouping. The catalog developed for our LELS sample will be made available online. The online table will include the photometric values and the estimated line EWs.

5. Conclusion

In this study, we present the spectroscopic information of 38,152 LELS, identified from the LAMOST DR6. Acquiring F0-M9 "STAR" data from LAMOST DR6, we utilized a custom Python routine developed with the `scipy.signal.findpeaks` parameter to isolate spectra containing Hα emission. As the next step, we separated the ELS into various sub-classes such as PtMS candidates, IR excess sources, Fe/Ge/Ke stars, and dMe stars. We employed photometric and spectroscopic methods to do the same.

We have obtained one of the largest homogeneous data sets of LELS in this study. After the SIMBAD crossmatch, a sample of 29,222 was found to be new detections. This includes 65 IR excess sources, 7899 Fe/Ge/Ke stars, 17,533 dMe stars, and 3725 PtMS candidates. The spatial distribution of our data suggested that the stars observed are in the anti-center direction, which is similar to what we observe in the early-type ELS work done by B. Shridharan et al. (2021). Also, over 89% of the stars observed were within 1 kpc. It has also been ascertained that PtMS star candidates are observed at much longer distances due to their size and high luminosity.

We also discussed the spectral features observed in various late-type stars, encompassing both absorption and emission lines. Studying the major spectral lines observed in a star helps us understand the chemical composition, active phenomena, and the physical properties of a star. For late-type stars, the major emission features observed in our sample are noted. Furthermore, the line strength of the major emission lines, which include Balmer lines, ionized Ca lines, Pa lines, etc., and its distribution over various spectral types were analyzed. The statistics revealed that we observe intense emission lines in young stars due to their youth and intense disk activity in these sources. We observed strong metallic absorption lines in the spectra of F-, G-, and K-type ELS. Further, we classified the stars into four groups based on the presence or absence of three major emission lines, namely Hα, Ca II K, and Ca II 8662 Å. Deeper studies in this direction will help us to understand the line formation scenarios in low-mass stars.

The distribution of stars over various spectral types is also discussed in this work. Even though the classifications are made for various groups of LELS, further studies on various groups are required for a better understanding of the various properties of these objects.

Acknowledgments

We express our gratitude to the reviewer for their valuable comments and suggestions, which have greatly enhanced the quality of this manuscript. We would like to thank the Center for Research, CHRIST (Deemed to be University), Bangalore, India for providing the necessary support. B.M. is grateful to the Centre for Research, CHRIST (Deemed to be University), Bangalore for the research grant (Seed Money project) to carry out the present project (SMSS-2335). This work has made use of data products from the Guo Shoujing Telescope (the Large Sky Area Multi-Object Fiber Spectroscopic Telescope, LAMOST), and data from the European Space Agency (ESA) mission Gaia (https://www.cosmos.esa.int/gaia), processed by the Gaia Data Processing and Analysis Consortium (DPAC, https://www.cosmos.esa.int/web/gaia/dpac/consortium). Funding for the DPAC has been provided by national institutions, in particular, the institutions participating in the Gaia Multilateral Agreement. We thank the SIMBAD database and the online VizieR library service for helping us with the literature survey and obtaining relevant data.

Appendix
Additional Data

Table A1
The Sample Table of LAMOST LELS Sources

LAMOST Desid	R.A.	Decl.	LAMOST SpT	Classification	Group	Name
LAMOST J080307.80+144949.5	120.782514	14.830419	dM0	dMe	B	LM-LEMC_102
LAMOST J202431.01+421605.0	306.1292289	42.2680711	G2	CTTS	C	LM-LEMC_10581
LAMOST J223304.19+234418.7	338.26746	23.738552	K5	Ke	C	LM-LEMC_10960
LAMOST J013356.31+294201.1	23.484628	29.700313	dM2	dMe	B	LM-LEMC_118
LAMOST J114044.45+310630.5	175.185241	31.108484	K7	Ke	B	LM-LEMC_122
LAMOST J223227.51+303416.0	338.114653	30.571131	dM5	dMe	B	LM-LEMC_13
LAMOST J181613.21+495205.2	274.0550637	49.8681296	dM6	dMe	A	LM-LEMC_1464
LAMOST J110134.88+320928.8	165.395343	32.158016	K7	Ke	B	LM-LEMC_149
LAMOST J111248.50+242320.4	168.202105	24.389021	G7	Ge	D	LM-LEMC_171
LAMOST J043749.67+514255.8	69.456969	51.715519	F0	Fe	D	LM-LEMC_201
LAMOST J121511.31+582749.5	183.797165	58.463768	K7	Ke	B	LM-LEMC_205
LAMOST J035034.14+275836.5	57.642273	27.976813	K7	Ke	B	LM-LEMC_21
LAMOST J052108.71-054229.0	80.286323	−5.708056	dM1	CTTS	A	LM-LEMC_2103
LAMOST J035603.23+351450.5	59.013466	35.247377	dM1	CTTS	A	LM-LEMC_2211
LAMOST J101432.90+300616.4	153.637106	30.104568	dM4	dMe	B	LM-LEMC_228
LAMOST J033233.00+310221.5	53.13753	31.039308	gM6	PtMS	A	LM-LEMC_2516
LAMOST J063949.01+101602.8	99.954237	10.267467	G5	PtMS	D	LM-LEMC_253
LAMOST J115740.34-011012.4	179.418112	−1.170133	dM5	dMe	D	LM-LEMC_267
LAMOST J063351.63+044942.8	98.465158	4.82856	F5	Fe	D	LM-LEMC_316
LAMOST J061439.96-062917.4	93.666512	−6.4881826	K1	Ke	A	LM-LEMC_3273
LAMOST J062920.78+044006.9	97.336599	4.668605	G3	Ge	D	LM-LEMC_375
LAMOST J221010.40+293625.8	332.543353	29.607178	K7	Ke	B	LM-LEMC_4
LAMOST J063321.38+050018.8	98.339094	5.005244	G5	PtMS	D	LM-LEMC_404
LAMOST J063416.41+044202.3	98.568391	4.700666	F2	Fe	D	LM-LEMC_405
LAMOST J033344.06+073142.8	53.433604	7.528561	dM0	dMe	B	LM-LEMC_41
LAMOST J063100.24+044738.2	97.751028	4.793951	K5	PtMS	D	LM-LEMC_425
LAMOST J063003.35+044349.6	97.513998	4.7304482	G6	Ge	D	LM-LEMC_439
LAMOST J004430.15+442703.6	11.125628	44.451011	K7	Ke	B	LM-LEMC_526
LAMOST J005822.58+291420.3	14.5941057	29.238974	K7	Ke	B	LM-LEMC_61
LAMOST J044049.50+255118.9	70.20628	25.855261	dM2	CTTS	B	LM-LEMC_612
LAMOST J054112.83+252912.2	85.303487	25.486748	dM4	dMe	B	LM-LEMC_647
LAMOST J025217.58+361648.1	43.073285	36.280052	K4	PtMS	A	LM-LEMC_664
LAMOST J235556.66+324013.2	358.986106	32.670338	F7	Fe	D	LM-LEMC_80
LAMOST J042951.55+260644.5	67.464831	26.112387	dM0	CTTS	A	LM-LEMC_861
LAMOST J053232.08+104417.9	83.133682	10.738327	dM4	CTTS	A	LM-LEMC_8805
LAMOST J034458.57+235541.0	56.244074	23.928062	dM5	dMe	A	LM-LEMC_8860
LAMOST J053411.38-045122.9	83.547457	−4.8563636	dM4	dMe	A	LM-LEMC_9595

ORCID iDs

B. Shridharan https://orcid.org/0000-0002-2585-0111
S. Nidhi https://orcid.org/0000-0003-2825-147X

References

Alcalá, J., Covino, E., Franchini, M., et al. 1993, A&A, 272, 225
Andre, P., Ward-Thompson, D., & Barsony, M. 1993, ApJ, 406, 122
Anusha, R., Mathew, B., Shridharan, B., et al. 2021, MNRAS, 501, 5927
Bailer-Jones, C., Rybizki, J., Fouesneau, M., Demleitner, M., & Andrae, R. 2021, AJ, 161, 147
Barentsen, G., Farnhill, H. J., Drew, J., et al. 2014, MNRAS, 444, 3230
Batalha, N. M., Borucki, W. J., Koch, D. G., et al. 2010, ApJL, 713, L109
Bidelman, W. P. 1954, ApJS, 1, 175
Bohannan, B. 1987, IUE Proposal, 2747
Brittain, S. D., Kamp, I., Meeus, G., Oudmaijer, R. D., & Waters, L. B. F. M. 2023, SSRv, 219, 7
Cacciari, C., & Freeman, K. 1983, ApJ, 268, 185, Part 1
Carpenter, J. M. 2001, AJ, 121, 2851
Chang, H.-Y., Song, Y.-H., Luo, A.-L., et al. 2017, ApJ, 834, 92
Charbonneau, P. 2014, ARA&A, 52, 251
Cincunegui, C., Diaz, R. F., & Mauas, P. J. D. 2007, A&A, 469, 309
Cram, L. 1989, Proc, ASA, 8, 2
Cutri, R., Wright, E., Conrow, T., et al. 2012, yCat, II/311
Delfosse, X., Forveille, T., Perrier, C., & Mayor, M. 1998, A&A, 331, 581
Deng, L.-C., Newberg, H. J., Liu, C., et al. 2012, RAA, 12, 735
Drew, J. E., Greimel, R., Irwin, M. J., et al. 2005, MNRAS, 362, 753
Eason, E. L., Giampapa, M., Radick, R., Worden, S., & Hege, E. 1992, AJ, 104, 1161
Eyer, L., Rimoldini, L., Audard, M., et al. 2019, A&A, 623, A110
France, K., Arulanantham, N., Fossati, L., et al. 2018, ApJS, 239, 16
Gillet, D. 1988, A&A, 192, 206
Gillet, D., Maurice, E., & Baade, D. 1983, A&A, 128, 384
Gizis, J. E., Reid, I. N., & Hawley, S. L. 2002, AJ, 123, 3356
Gras-Velázquez, À., & Ray, T. 2005, A&A, 443, 541
Green, G. 2018, JOSS, 3, 695
Groenewegen, M. 2012, A&A, 540, A32
Guo, Y.-X., Yi, Z.-P., Luo, A.-L., et al. 2015, RAA, 15, 1182
Hall, J. C. 2008, LRSP, 5, 1
Hartmann, L., Herczeg, G., & Calvet, N. 2016, ARA&A, 54, 135
Hartmann, L., Hewett, R., & Calvet, N. 1994, ApJ, 426, 669
Henize, K. 1976, ApJS, 30, 491
Herbst, W., & Miller, J. R. 1989, AJ, 97, 891
Hilton, E. J., West, A. A., Hawley, S. L., & Kowalski, A. F. 2010, AJ, 140, 1402
Houdebine, E., Doyle, J., & Koscielecki, M. 1995, A&A, 294, 773
Joy, A. H., & Abt, H. A. 1974, ApJS, 28, 1
Koenig, X., & Leisawitz, D. 2014, ApJ, 791, 131
Kogure, T., & Leung, K.-C. 2010, The Astrophysics of Emission-line Stars, 342 (Berlin: Springer)
Kurosawa, R., Harries, T. J., & Symington, N. 2005, Protostars and Planets V, 8412 (Tucson, AZ: Univ. Arizona Press)
Lada, C. J. 1987, in Star Forming Region, Vol. 115 ed. M. Peimbert & J. Jugaku, 1
Le Coarer, E., Rosado, M., Georgelin, Y., & Viale, A. 2005, New Aspects of Magellanic Cloud Research: Proc. Second European Meeting on the Magellanic Clouds Organized by the Sonderforschungsbereich 328 "Evolution of Galaxies" (Berlin: Springer), 77
Li, J., FELLOW, L., Liu, C., et al. 2019, ApJ, 874, 138
Lima, G., Alencar, S., Calvet, N., Hartmann, L., & Muzerolle, J. 2010, A&A, 522, A104
Liu, C., Deng, L.-C., Carlin, J. L., et al. 2014, ApJ, 790, 110
Lockwood, G. W., Skiff, B. A., Henry, G. W., et al. 2007, ApJS, 171, 260
López-Santiago, J., Montes, D., Gálvez-Ortiz, M., et al. 2010, A&A, 514, A97
MacConnell, D. 1981, A&AS, 44, 387
Martayan, C., Baade, D., & Fabregat, J. 2010, A&A, 509, A11
Martínez, R. R., Lopez, L. A., Shappee, B. J., et al. 2020, ApJ, 892, 144
Merrill, P. W., & Burwell, C. G. 1933, ApJ, 78, 87
Meyer, M. R., Calvet, N., & Hillenbrand, L. A. 1997, AJ, 114, 288
Meyssonnier, N., & Azzopardi, M. 1993, A&AS, 102, 451
Morin, J. 2012, EAS, 57, 165
Mould, J., & Wallis, R. 1977, MNRAS, 181, 625
Muzerolle, J., Calvet, N., & Hartmann, L. 1998a, ApJ, 492, 743
Muzerolle, J., Hartmann, L., & Calvet, N. 1998b, AJ, 116, 455
Newton, E. R., Irwin, J., Charbonneau, D., et al. 2017, ApJ, 834, 85
Nidhi, S., Mathew, B., Shridharan, B., et al. 2023, JApA, 44, 75
Pace, G., Melendez, J., Pasquini, L., et al. 2009, A&A, 499, L9
Padgett, D. L., Cieza, L., Stapelfeldt, K. R., et al. 2006, ApJ, 645, 1283
Prusti, T., De Bruijne, J., Brown, A. G., et al. 2016, A&A, 595, A1
Radick, R. R., Wilkerson, M., Worden, S., et al. 1983, PASP, 95, 300
Reiners, A., Joshi, N., & Goldman, B. 2012, AJ, 143, 93
Robinson, R. D., Cram, L. E., & Giampapa, M. S. 1990, ApJS, 74, 891
Ruiz-Dern, L., Babusiaux, C., Arenou, F., Turon, C., & Lallement, R. 2018, A&A, 609, A116
Shridharan, B., Mathew, B., Nidhi, S., et al. 2021, RAA, 21, 288
Singh, R., Reddy, B. E., Kumar, Y. B., & Antia, H. 2019, ApJL, 878, L21
Skrutskie, M., Cutri, R., Stiening, R., et al. 2006, AJ, 131, 1163
Smith, G. 2011, Obs, 131, 1
Steinmetz, M. 2002, astro-ph/0211417
Stephenson, C. 1986, ApJ, 300, 779
Suárez Mascareño, A., Rebolo, R., González Hernández, J., & Esposito, M. 2015, MNRAS, 452, 2745
Sun, Y., Cheng, Z., Ye, S., et al. 2021, ApJS, 257, 65
Traven, G., Zwitter, T., Van Eck, S., et al. 2015, A&A, 581, A52
Vallenari, A., Brown, A., Prusti, T., et al. 2023, A&A, 674, A1
Vasu Mallik, S. 1982, JApA, 3, 39
Vaughan, A. H., & Preston, G. W. 1980, PASP, 92, 385
Welsh, B. Y., Wheatley, J. M., Seibert, M., et al. 2007, ApJS, 173, 673
West, A. A., Hawley, S. L., Walkowicz, L. M., et al. 2004, AJ, 128, 426
Wilson, T. J., Matt, S., Harries, T., & Herczeg, G. 2022, MNRAS, 514, 2162
Wiramihardja, S. D., Kogure, T., Yoshida, S., Ogura, K., & Nakano, M. 1989, PASJ, 41, 155
Wood, P. 1979, ApJ, 227, 220, Part 1
Wray, J. D. 1966, AJ, 71, 403
Wu, Y., Du, B., Luo, A., Zhao, Y., & Yuan, H. 2014, Proc. Int. Astronomical Union, 10 (Cambridge: Cambridge Univ. Press), 340
Yan, H., Li, H., Wang, S., et al. 2022, Innov, 100224
Yao, Y., Liu, C., Deng, L., De Grijs, R., & Matsunaga, N. 2017, ApJS, 232, 16
Yi, Z., Chen, Z., Pan, J., et al. 2019, ApJ, 887, 241
Yi, Z., Luo, A., Song, Y., et al. 2014, AJ, 147, 33
York, D. G., Adelman, J., Anderson, J. E., Jr., et al. 2000, AJ, 120, 1579
Young, A., & Koniges, A. 1977, ApJ, 211, 836, Part 1
Young, A., Skumanich, A., Stauffer, J. R., Bopp, B. W., & Harlan, E. 1989, ApJ, 344, 427
Žerjal, M., Zwitter, T., Matijevič, G., et al. 2017, ApJ, 835, 61
Zhang, B., Liu, C., & Deng, L.-C. 2020, ApJS, 246, 9
Zhao, G., Zhao, Y.-H., Chu, Y.-Q., Jing, Y.-P., & Deng, L.-C. 2012, RAA, 12, 723
Zhong, J., Lépine, S., Li, J., et al. 2015, RAA, 15, 1154